Chinese Chemical Letters 37 (2026) 112482

Contents lists available at ScienceDirect

Chinese Chemical Letters

journal homepage: www.elsevier.com/locate/cclet

MOFs-derived Ru/MoO_x–TiO_2 catalyst for photothermal synergistic catalytic elimination of multi-component VOCs

Xun Wang[a,b], Zeya Li[a], Ruyi Gao[c], Ying Feng[a], Zhiquan Hou[a], Zhiwei Wang[a], Zhen Wei[a], Yuxi Liu[a], Hongxing Dai[a], Jiguang Deng[a,*]

[a] State Key Laboratory of Materials Low-Carbon Recycling, College of Materials Science and Engineering, Beijing University of Technology, Beijing 100124, China
[b] School of Resource and Environment, Linyi University, Linyi 276002, China
[c] School of Resource & Environment and Safety Engineering, Jining University, Qufu 273155, China

ARTICLE INFO

Article history:
Received 17 December 2025
Revised 28 January 2026
Accepted 30 January 2026
Available online 17 July 2026

Keywords:
Multi-component VOCs
MOF-derived catalyst
MoO_x doping
Photothermal catalytic oxidation
Synergy mechanism

ABSTRACT

A highly efficient and energy-saving photothermal synergistic catalytic oxidation technology was developed to eliminate ethyl acetate (EA) and 1,2-dichloroethane (1,2-DCE) over MoO_x–TiO_2, derived by MIL-125(Ti), supported Ru catalysts (Ru/MoO_x–TiO_2). The introduction of MoO_x enhanced the light absorption capacity, carrier separation capacity and redox capacity of the catalyst, thus significantly improving the photothermal synergistic catalytic performance, with Ru/MoO_x–TiO_2 exhibiting outstanding activity for EA and 1,2-DCE oxidation ($T_{90\,\%}$ = 212 and 319 °C, respectively). Meanwhile, the abundant Brønsted acidic sites on Ru/MoO_x–TiO_2 were inclined to generate more HCl and CO_2, and reduce the release of chlorine-containing byproducts than that over Ru/TiO_2. The characterization results by the *in situ* XPS, *in situ* PL and *in situ* EPR exhibited that the improvement of the photothermal synergistic catalytic oxidation performance was attributed to the coupling effect between electron migration on the catalyst surface and active oxygen species during the photothermal synergistic catalytic reaction process. This work has provided a promising path for simultaneously enhancing the removal efficiency of multi-component VOCs and the selectivity of target products.

© 2026 Published by Elsevier B.V. on behalf of Chinese Chemical Society and Institute of Materia Medica, Chinese Academy of Medical Sciences.

Oxygenated and chlorinated VOCs (OVOCs and CVOCs) emissions are involved in numerous industries, and pose a serious threat to the environment and human health because of the strong water solubility or high toxicity, stable chemical properties and difficulty in degradation [1–3]. To meet the increasingly strict VOCs emission standards, the treatment technologies can be coupled to achieve coordinated reduction of pollution and carbon. The photothermal synergistic catalytic oxidation technology is capable of simultaneously avoiding the problems of high energy consumption of catalytic oxidation and low efficiency of photocatalytic oxidation. The photothermal synergistic effect will significantly improve the removal efficiency of VOCs and has a promising application prospect [4,5]. Nevertheless, due to the differences in the physicochemical properties of VOCs and reaction conditions, there are still large gaps in the in-depth research on the synergistic effect of photothermal catalytic oxidation.

Metal-organic frameworks (MOFs) have been extensively utilized in the field of VOCs elimination owing to its abundant catalytic oxidation sites, large porosity and specific surface area [6]. Unfortunately, the stability of most MOFs is poor, which leads to its inability to meet the requirements for the efficient removal of refractory or multi-component VOCs [7]. MOFs derivatives, prepared by high-temperature calcination in a specific atmosphere (air, nitrogen or helium, *etc.*) using MOFs as precursors, can not only inherit the high specific surface area and pore structure of its precursor MOFs, but also possess higher stability and activity, expanding their application [8,9]. At present, MOF-derivatives (such as TiO_2 derived from MIL-125, MnO_x derived from Mn-BTC, Pd@ZrO_2 derived from UIO-66) have been used for catalytic oxidation of ethyl acetate, toluene and acetone, while there are relatively few reports on the removal of CVOCs (MnO_x/Co_3O_4 derived from Mn/ZIF-67 and MnO_x derived from Mn-MOF-74 were used to remove chlorobenzene) [5,10–12]. Considering the advantages of MOF-derivatives in removal gas pollutant, it is highly demanded for the development of MOF-derivatives for the photother-

* Corresponding author.
E-mail address: jgdeng@bjut.edu.cn (J. Deng).

https://doi.org/10.1016/j.cclet.2026.112482
1001-8417/© 2026 Published by Elsevier B.V. on behalf of Chinese Chemical Society and Institute of Materia Medica, Chinese Academy of Medical Sciences.

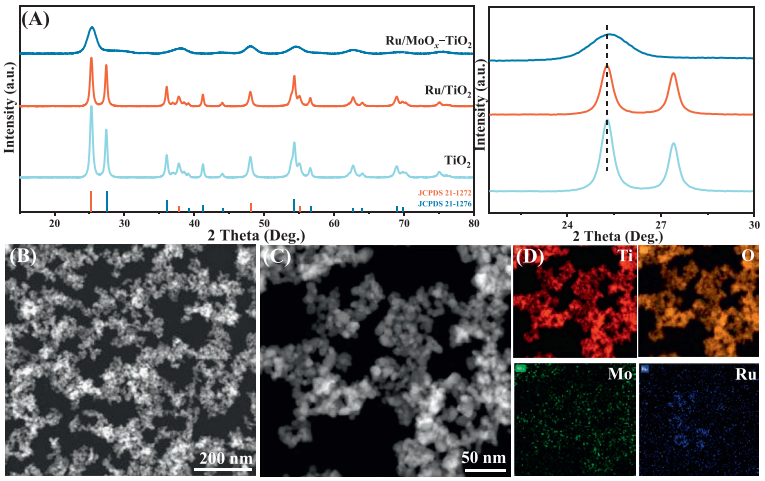


Fig. 1. (A) XRD patterns of TiO_2, Ru/TiO_2 and Ru/MoO_x–TiO_2. (B, C) TEM images and (D) EDS elemental mappings of Ru/MoO_x–TiO_2.

mal synergistic catalytic oxidation of multi-component VOCs containing CVOCs.

In the process of removing multi-component VOCs, it is indispensable to simultaneously enhance catalytic activity and the selectivity of target products [13]. Especially when the system contains CVOCs, the production of polychlorinated byproducts should be minimized as possible. Generally speaking, the regulation of the Brønsted acidic site can effectively inhibit the occurrence of highly toxic chlorine-containing byproducts and tent to produce the relatively desirable product (HCl) in the oxidation of CVOCs [14,15]. A lot of reports have shown that the supported Ru catalysts exhibit excellent resistance to chlorine poisoning, because the Cl species produced by the cleavage of C-Cl bond can be efficiently removed from the catalyst surface [16–18]. Since the unfilled d electron orbitals are conducive to promoting the adsorption and activation of VOCs on the catalyst surface, the presence of Mo species has the potential to enhance the catalytic activity [19]. Moreover, doping Mo can regulate the Brønsted acid sites of the catalyst, which inhibit desorption of chlorine-containing byproducts [20,21]. Here, we introduce the MoO_x species into the TiO_2 supported Ru catalyst, derived from MIL-125(Ti), and explored the photothermal synergistic catalytic oxidation performance for the typical multicomponent VOCs (EA and 1,2-DCE). Series *in situ* characterization techniques were used to investigate the mechanism of photothermal synergistic effect. In addition, the positive role of MoO_x in improving photothermal catalytic activity and product selectivity was also probed.

All of the chemicals utilized in the studies were of analytical pure and used without further purification. And the detailed information of the chemicals, catalyst preparation, characterization methods and catalytic performance measurement were shown in Texts S1-S4 (Supporting information).

As shown in Fig. S1A (Supporting information), the X-ray diffraction (XRD) patterns of Ru/MIL-125 and Ru/Mo–MIL-125 were consistent with that of MIL-125, indicating the introduction of Ru and Mo had little effect on the crystal phase of MIL-125. From the X-ray photoelectron spectroscopy (XPS) spectra of O 1s (Fig. S1B in Supporting information), O–Mo (530.5 eV) can be only observed in Ru/Mo-MIL-125 [22]. In Figs. S1C, D and S2 (Supporting information), the morphology of Ru/Mo-MIL-125 was basically kept, and the Mo species were uniformly distributed. These results indicated that part of Ti was successfully replaced by Mo, without the change in the structure of MIL-125.

The XRD patterns of TiO_2, Ru/TiO_2 and Ru/MoO_x–TiO_2 obtained after calcination were shown in Fig. 1A. Compared with TiO_2, the introduction of Mo would cause the phase transition of anatase TiO_2 and rutile TiO_2, manifested as the disappearance of the (110) and (101) crystal planes of rutile TiO_2 in Ru/MoO_x–TiO_2. In addition, no characteristic peaks belonging to MoO_x and Ru species were observed, which might be related to the uniform distribution of MoO_x and Ru species. From the locally magnified XRD patterns, the diffraction peaks did not shift when Ru was present, indicating the Ru was introduced *via* the loading way. Ru/MoO_x–TiO_2 appeared granular (Fig. 1B), and the Mo, Ru species were highly dispersed (Figs. 1C and D).

As representatives of typical OVOCs and CVOCs, EA and 1,2-DCE were selected to evaluate the photothermal catalytic oxidation activity of the as-prepared catalysts. As shown in Figs. S3 and S4 (Supporting information), the same theoretical loading of Ru (0.3 wt%) was adopted for the different supports. The photothermal catalytic activity for EA and 1,2-DCE oxidation over Ru/TiO_2 were both higher than those on Ru/commercial TiO_2. Especially at 280 °C and 300 °C, the conversion of EA on Ru/TiO_2 were 48 % and 72.9 % respectively, while that was only 21.1 % and 42.0 % on Ru/commercial TiO_2. Based on the TGA results, the catalytic activity of Ru/Mo-MIL-125 was investigated below 380 °C. Ru/Mo-MIL-125 exhibited higher $T_{90\,\%}$ for EA and 1,2-DCE oxidation than Ru/MoO_x–TiO_2. The above results demonstrated the superiority of TiO_2 derived from MIL-125(Ti). As can be seen from Fig. S5 (Supporting information), the catalytic activity for photothermal elimination of EA was improved with the increase in Mo content, while the 1,2-DCE oxidation was enhanced when the content of Mo increased to 10.2 wt% and gradually declined as the content of Mo continued to augment. XRD patterns (Fig. S5C) showed when the content of Mo increased to 15.1 wt%, the diffraction peaks of MoO_3 appeared due to phase separation [23]. Hence, the MoO_x–TiO_2 samples with actual Mo loading of 10.2 wt% was selected to explore the photothermal catalytic performance for EA and 1,2-DCE oxidation.

As shown in Fig. 2A and Table S1 (Supporting information), it could be seen that there was a sharp increase in EA conversion after the introduction of MoO_x, with $T_{50\,\%}$ and $T_{90\,\%}$ dropping to 193 and 228 °C, respectively. The Ru/MoO_x–TiO_2 catalyst exhibited the most outstanding photothermal catalytic activity for EA oxidation. The order in specific reaction rates for EA oxidation was TiO_2 < Ru/TiO_2 < MoO_x–TiO_2 < Ru/MoO_x–TiO_2, consistent with the order of photothermal catalytic oxidation activity. For the photothermal catalytic oxidation of 1,2-DCE (Fig. 2B), Ru/MoO_x–TiO_2 also shown the best catalytic oxidation activity. The above results indicated that Ru and MoO_x were the active sites for the catalytic oxida-

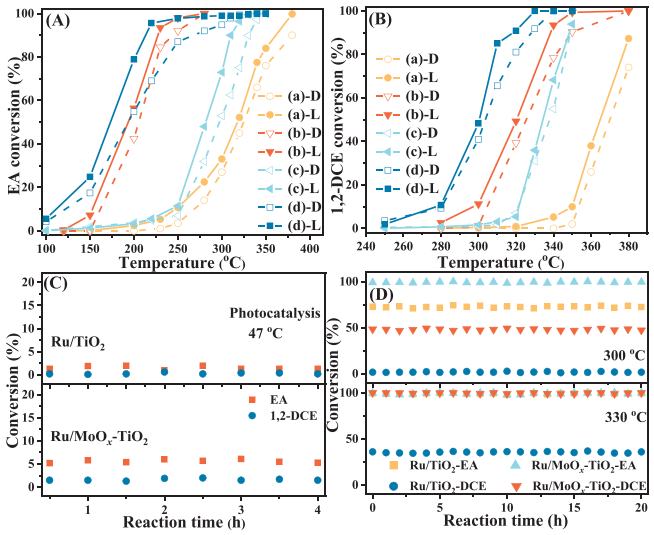


Fig. 2. (A) EA and (B) 1,2-DCE conversion as a function of temperature for the oxidation of mixed VOCs over the (a) TiO_2, (b) MoO_x–TiO_2, (c) Ru/TiO_2 and (d) Ru/MoO_x–TiO_2 catalysts under light irradiation (-L) or in the dark (-D). (C) Photocatalytic activities for EA and 1,2-DCE oxidation over the Ru/TiO_2 and Ru/MoO_x–TiO_2 catalysts, and (D) catalytic stability test for mixed VOCs oxidation over the Ru/TiO_2 and Ru/MoO_x–TiO_2 catalysts. Reaction conditions: 1000 ppm EA, 500 ppm 1,2-DCE, 20 vol% O_2, balanced with N_2, UV–vis-IR, and 200 mW/cm^2.

tion of EA and 1,2-DCE. Compared to TiO_2 and Ru/TiO_2, MoO_x–TiO_2 showed larger change in terms of $T_{90\,\%}$ and specific reaction rate, and MoO_x was speculated as the dominant active site. It was worth mentioning that in the catalytic oxidation of the VOCs mixture, the catalytic activity of TiO_2, MoO_x–TiO_2, Ru/TiO_2 and Ru/MoO_x–TiO_2 were improved to different extents after the addition of light. In particular, over Ru/MoO_x–TiO_2 at 220 °C, EA was almost eliminated under the photothermal catalytic reaction, but only 69 % of EA was oxidized under the thermocatalytic reaction. Similar phenomena could also be observed for 1,2-DCE oxidation. Furthermore, the conversion of EA and 1,2-DCE over Ru/MoO_x–TiO_2 at 47 °C were always <6 % within 4-h reaction time under the photocatalytic condition (Fig. 2C), indicated that the light-driven thermal catalytic oxidation could be negligible. The stability of the catalyst was an important indicator for practical application. As shown in Fig. 2D, whether at high conversion or low conversion, Ru/TiO_2 and Ru/MoO_x–TiO_2 demonstrated excellent stability for EA and 1,2-DCE oxidation within 20 h reaction time. The XRD (Fig. S6A in Supporting information) and XPS spectra (Figs. S6B-F in Supporting information) indicated that the crystal phase structure, surface elemental composition, and metal chemical state of Ru/MoO_x–TiO_2 were not changed after the catalytic stability evaluation at 330 °C. Specially, the chlorine contents over Ru/TiO_2 was 3.6 times higher than that over Ru/MoO_x–TiO_2. The presence of MoO_x could effectively reduce the chlorine deposition on the catalyst surface and prevent catalyst deactivation. Besides, industrial emissions would contain H_2O, which may influence catalytic activity [24]. As shown in Fig. S7 (Supporting information), the contained water vapor had little effect on the catalytic oxidation of EA, nevertheless, the conversion of 1,2-DCE oxidation was decreased. After cutting off the water vapor, the photothermal catalytic activity returned to the initial level, indicating that the decrease in activity caused by water vapor was reversible.

Not to be overlooked, different VOCs would interact with each other during the oxidation process. So, we further investigated the photothermal synergistic catalytic performance of the catalysts for the oxidation of EA, 1,2-DCE, and the mixed VOCs (Figs. S8A and B in Supporting information). When the system contained multi-component VOCs, the conversion of EA and 1,2-DCE were all suppressed, with the inhibition of photothermal catalytic activity for 1,2-DCE elimination being more obvious in the presence of EA. It was worth emphasizing that whether in the catalytic oxidation of single VOCs or multi-component VOCs, Ru/MoO_x–TiO_2 exhibited superior synergistic photothermal catalytic performance compared to Ru/TiO_2. The VOCs-TPD results (Fig. S8C in Supporting information) showed that the decline in the catalytic activity for EA and 1,2-DCE oxidation in the mixture was might related to the competitive adsorption on the catalyst surface.

The presence of MoO_x significantly enhanced the catalytic activity. Therefore, the influence of MoO_x on the redox property of the catalyst was explored, as shown in Fig. S9 (Supporting information). When MoO_x was present, an extra reduction peak appeared at 86 °C, and the reduction peaks shifted towards lower temperature, indicating an improvement in reducibility. In Fig. S9B, the oxygen desorption area over Ru/MoO_x–TiO_2 was larger than that over Ru/TiO_2, which was conducive to the deep oxidation of VOCs. The O_{ads}/O_{latt} (530.8 eV/530.1 eV) molar ratio of Ru/MoO_x–TiO_2 (0.32) were higher than that of Ru/TiO_2 (0.16) (Fig. S9C), which played a promoting role in photothermal catalytic activity [25]. VOCs-TPD technology (Fig. S10 in Supporting information) showed that the desorption of EA and 1,2-DCE over Ru/MoO_x–TiO_2 was larger than that over Ru/TiO_2, indicated that the Ru/MoO_x–TiO_2 possessed a larger VOCs adsorption capacity. Fig. S11 (Supporting information) displayed that Ru/MoO_x–TiO_2 had the stronger light absorption capacity, especially in the range of 400–800 nm, and photo-generated carrier separation ability, thus generating more reactive oxygen species ($^{\bullet}O_2^-$ and $^{\bullet}OH$) to directly participate in the photothermal catalytic reaction (Figs. S12 and S13 in Supporting information) [26,27]. Therefore, the photothermal catalytic oxidation ability of Ru/MoO_x–TiO_2 for EA and 1,2-DCE was superior to that of Ru/TiO_2.

In addition to enhancing the photothermal catalytic oxidation activity, the presence of MoO_x may also have an impact on the product distribution. As could be seen from Fig. S14 (Supporting information), $CHCl_3$ was only observed over Ru/TiO_2 at $T_{90\,\%}$. Quantitative results (Figs. 3A-C and Fig. S15 in Supporting information) showed that for Ru/TiO_2, the maximum concentration of $C_2H_2Cl_2$ and $CHCl_3$ were 12.5 and 34.5 ppmv, which was much higher than that over Ru/MoO_x–TiO_2 (4.0 ppmv, not detected). Similarly, TPSR-MS profiles could also draw the above conclusion. Ru/MoO_x–TiO_2 displayed stronger HCl, CH_3COOH and CO_2 desorption peaks, and weaker $CHCl_3$ and Cl_2 desorption peaks (Figs. 3D-F and Fig. S16 in Supporting information). The selectivity to the chlorine-containing product was shown in Fig. 4A. Ru/MoO_x–TiO_2 exhibited a higher HCl selectivity, reaching 98 %, while the HCl selectivity over Ru/TiO_2 was only 86 %. Moreover, the selectivity of $CHCl_3$ over Ru/TiO_2 was calculated to be 12 %, which was not observed over Ru/MoO_x–TiO_2. Based on the above results, it could be concluded that the introduction of Mo could reduce the formation of chlorine-containing byproducts such as $CHCl_3$, CH_2Cl_2, and Cl_2, and improve the selectivity of HCl and CO_2.

The Brønsted and Lewis acid sites of Ru/TiO_2 and Ru/MoO_x–TiO_2 catalysts were investigated by NH_3-*in situ* DRITFS and H_2O-TPD technology. The peak area of the Brønsted acid sites (1410 cm^{-1}) and Lewis acid sites (1100 cm^{-1}) of Ru/MoO_x–TiO_2 was larger than that of Ru/TiO_2, which indicated that the introduction of MoO_x could increase the Lewis acid sites, especially the Brønsted acid sites (Fig. 4B) [28,29]. The H_2O-TPD characterization further confirmed the result, as shown in Fig. 4C. Ru/MoO_x–TiO_2 had stronger dehydration strength of type II H_2O (150–300 °C), which guaranteed enough H and H_2O reacted with the dissociated Cl. Moreover, type II H_2O was also associated with the Brønsted acid sites of the catalyst [30,31]. Therefore, the abundance of Brønsted acid sites, due to the presence of MoO_x in

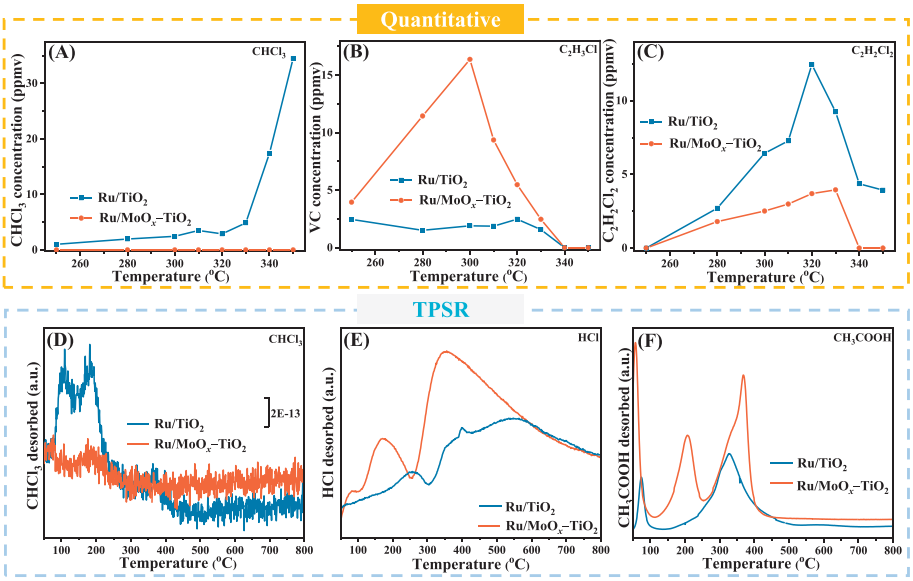


Fig. 3. (A-C) Product distribution in the photothermal catalytic oxidation of the multi-component VOCs, and (D) $CHCl_3$, (E) HCl, and (F) CH_3COOH desorption in the TPSR profiles over $Ru/MoO_x–TiO_2$ and Ru/TiO_2.

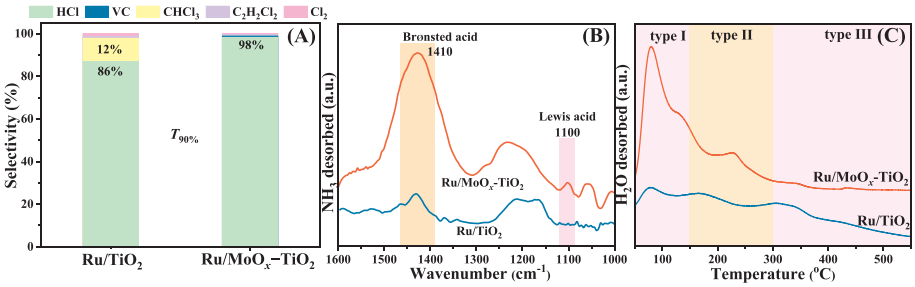


Fig. 4. (A) Selectivity of chlorine-containing product over Ru/TiO_2 and $Ru/MoO_x–TiO_2$ at the temperature required for 90 % conversion of 1,2-DCE. (B) *In situ* DRIFTS spectra of NH_3 adsorption and (C) H_2O-TPD profiles over Ru/TiO_2 and $Ru/MoO_x–TiO_2$.

$Ru/MoO_x–TiO_2$, not only enhanced the selectivity to HCl, but also reduced the generation of chlorine-containing by-products. According to the results of *in situ* DRIFTS (Fig. S17 in Supporting information), VOCs-TPSR and GC–MS, it could be found that the introduction of MoO_x had little effect on the reaction pathway of the catalytic oxidation, that is, the excellent photothermal catalytic oxidation activity of $Ru/MoO_x–TiO_2$ was not due to the change in the reaction process. The oxidation mechanism of EA and 1,2-DCE had also been inferred (Fig. S18 in Supporting information).

In order to explore the photothermal synergistic effect, a series of *in situ* characterization technologies have been developed. Compared with the dark condition, the peaks of the Mo 3d XPS spectrum moved towards the low binding energy, while the peaks of the Ru 3d XPS spectrum moved towards the high binding energy, indicating that Mo gained electrons and Ru lost electrons, and there was electron transfer between Mo and Ru under irradiation (Figs. 5A, B and Fig. S19 in Supporting information). It could be seen that as the temperature rose, the photoluminescence (PL) peak intensity gradually decreased (Fig. S20 in Supporting information), indicating that the increase in temperature was beneficial for the separation of photo-generated electrons and holes. Besides, the signals of $^{\bullet}O_2^-$ and $^{\bullet}OH$ over $Ru/MoO_x–TiO_2$ were gradually heightened with the increase of temperature (Figs. 5C and D), indicating that the increase of temperature was conducive to the generation of reactive oxygen species. Therefore, the improvement of photothermal catalytic oxidation performance was due to the photothermal synergistic effect. $Ru/MoO_x–TiO_2$ exhibited excellent redox capacity and the relatively high adsorbed oxygen concentration, leading to the improvement of photothermal catalytic oxidation activity. On the other hand, there was electron transfer

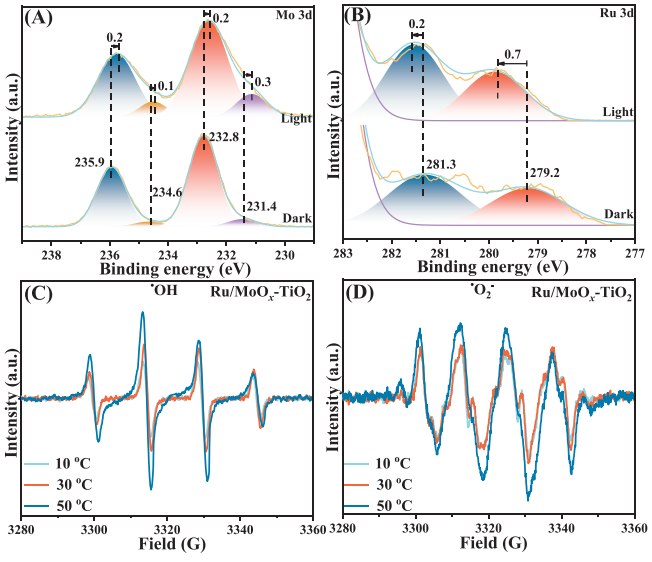


Fig. 5. (A) Mo 3d and (B) Ru 3d XPS spectra of $Ru/MoO_x–TiO_2$ under dark or light condition. EPR spectra of (C) $^{\bullet}O_2^-$ and (D) $^{\bullet}OH$ active radicals on $Ru/MoO_x–TiO_2$ at different temperature.

between Mo and Ru under irradiation, which inhibited the recombination of photo-generated electrons and holes, and be beneficial for generating of $^{\bullet}O_2^-$ and $^{\bullet}OH$. As the temperature rose, it was also conducive to accelerating the migration speed of photo-generated carriers.

In conclusion, the Ru/MoO_x–TiO_2 catalyst was prepared by the one-pot method using MIL-125(Ti) as the precursor. *In situ* MoO_x doping enhanced the light absorption capacity, photo-generated carrier utilization capacity, and REDOX capacity of the catalyst to improve the photothermal catalytic oxidation activity, and endowed the catalyst with more Brønsted acidic sites, reducing the generation of chlorine-containing by-products and enhancing the selectivity of the ideal product. The photothermal synergistic effect, attributed to the coupling between electron migration on the catalyst surface and active oxygen species under irradiation conditions, had enhanced the catalytic oxidation efficiency and reduced the required reaction temperature. The present study provided an efficient and environmentally friendly approach for the mixed VOCs elimination.

CRediT authorship contribution statement

Xun Wang: Writing – original draft, Methodology, Investigation, Formal analysis, Data curation. **Zeya Li:** Writing – original draft, Investigation, Data curation. **Ruyi Gao:** Investigation, Formal analysis, Data curation. **Ying Feng:** Validation, Formal analysis, Data curation. **Zhiquan Hou:** Writing – original draft, Methodology, Formal analysis. **Zhiwei Wang:** Visualization, Investigation, Formal analysis. **Zhen Wei:** Writing – original draft, Validation, Formal analysis. **Yuxi Liu:** Writing – review & editing, Supervision. **Hongxing Dai:** Writing – review & editing, Supervision. **Jiguang Deng:** Writing – review & editing, Supervision, Project administration, Conceptualization.

Declaration of competing interest

The authors declare that they have no known competing financial interests or personal relationships that could have appeared to influence the work reported in this paper.

Acknowledgments

This work was financially supported by the National Key R&D Program of China (No. 2023YFB3810801), National Natural Science Foundation of China (Nos. 22425601 and U23A20120), and Beijing Nova Program (No. 20240484659).

Supplementary materials

Supplementary material associated with this article can be found, in the online version, at doi:10.1016/j.cclet.2026.112482.

References

[1] C. He, J. Cheng, X. Zhang, et al., Chem. Rev. 119 (2019) 4471–4568.
[2] R.Y. Gao, M.C. Zhang, Y.X. Liu, et al., Environ. Sci. Technol. 56 (2022) 9672–9682.
[3] Y. Xin, L. Cheng, Y.N. Lv, et al., ACS Catal. 12 (2022) 397–410.
[4] X. Wang, Z.Y. Li, R.Y. Gao, et al., Environ. Sci. Technol. 58 (2024) 17190–17200.
[5] X. Wang, L.K. Wu, Z.W. Wang, et al., Appl. Catal. B 322 (2023) 122075.
[6] G.Q. Fang, F.F. Wei, J. Lin, et al., J. Am. Chem. Soc. 145 (2023) 13169–13180.
[7] Y. Ma, L. Wang, J.Z. Ma, et al., ACS Catal. 11 (2021) 6614–6625.
[8] X.J. Li, F. Wang, Y.L. Dong, S.H. Ho, C.C. Wang, Environ. Sci. Ecotechnol. 29 (2026) 100650.
[9] G.C. Liu, X.Y. Liu, X.H. Yi, et al., Water Res. 289 (2026) 124791.
[10] F.K. Bi, Z.Y. Zhao, Y. Yang, et al., Environ. Sci. Technol. 56 (2022) 17321–17330.
[11] Z.L. Tang, Y.L. Wang, J. Xiong, et al., Appl. Catal. B 381 (2026) 125872.
[12] Z.Y. Hu, J. Chen, D.X. Yan, et al., Appl. Surf. Sci. 551 (2021) 149453.
[13] T. Wang, J.C. Cao, J. Li, D.D. Li, Z.M. Ao, Chin. Chem. Lett. 36 (2025) 110078.
[14] Q.P. Sun, X.H. Yu, L.K. Wu, et al., Environ. Sci. Technol. 58 (2024) 12719–12730.
[15] X.H. Yu, L.Y. Dai, Y. Peng, et al., Environ. Sci. Technol. 55 (2021) 14906–14916.
[16] Z.Y. Jiang, Y.D. Wang, C.W. Chen, C. He, Chin. Chem. Lett. 35 (2024) 109400.
[17] L. Wei, Y.X. Liu, S.P. Cui, et al., Adv. Funct. Mater. 33 (2023) 2306129.
[18] X.H. Yu, L.Y. Dai, J.G. Deng, et al., J. Catal. 400 (2021) 310–324.
[19] M. Liu, G.C. Lv, H. Liu, et al., Chin. Chem. Lett. 35 (2024) 108459.
[20] L.K. Wu, Y.X. Liu, X.H. Yu, et al., Environ. Sci. Technol. 59 (2024) 945–955.
[21] H. Zhang, X.H. Gao, B.W. Gong, et al., Appl. Catal. B 310 (2022) 121240.
[22] Y.Y. Wu, H.D. Ji, Q.M. Liu, et al., J. Hazard. Mater. 424 (2022) 127563.
[23] W.B. Pei, L.Y. Dai, Y.X. Liu, et al., J. Catal. 385 (2020) 274–288.
[24] Z.C. Zhang, R.X. Mei, F.X. Wang, et al., Environ. Sci. 12 (2025) 4843–4849.
[25] X.H. Yu, J.G. Deng, Y.X. Liu, et al., Environ. Sci. Technol. 56 (2022) 11739–11749.
[26] Y. Feng, L.Y. Dai, Z.W. Wang, et al., Environ. Sci. Technol. 56 (2022) 8722–8732.
[27] Y. Chai, F. Wang, Y. Gao, et al., Environ. Res. 282 (2025) 122099.
[28] J.P. Du, J.L. Chen, Y.L. Shan, et al., Chin. Chem. Lett. 36 (2025) 110019.
[29] X. Zhang, L.Y. Dai, Y.X. Liu, et al., Catal. Sci. Technol. 10 (2020) 3755–3770.
[30] L.K. Wu, Y.X. Liu, Y.W. Jia, et al., Appl. Catal. B 378 (2025) 125557.
[31] F.W. Lin, Z.M. Zhang, N. Li, et al., Chem. Eng. J. 404 (2021) 126534.